Interactions of nanobubbles with bovine serum albumin and papain films on gold surfaces

Viliam Kolivoška,[a)] Miroslav Gál, Magdaléna Hromadová, Štěpánka Lachmanová, and Lubomír Pospíšil

J. Heyrovský Institute of Physical Chemistry of ASCR, v.v.i., Dolejškova 3, 182 23 Prague, Czech Republic

Nanobubbles formed on monocrystalline gold/water interface by means of the ethanol-to-water solvent exchange were exposed to the solutions of either bovine serum albumin or papain proteins. Both proteins do not change the position of nanobubbles in water, as observed by *in situ* tapping mode atomic force microscopy imaging before and after the introduction of the protein. The aqueous environment was subsequently replaced by ethanol. While all nanobubbles were found to dissolve in ethanol in the presence of bovine serum albumin, most of them survived when papain was employed. The protective ability of papain was ascribed to its resistance towards the protein denaturation in aqueous solutions of ethanol. The authors employed *in situ* atomic force nanolithography to investigate the nanomorphology of the papain/nanobubble assemblies in ethanol. © *2011 American Vacuum Society*. [DOI: 10.1116/1.3650300]

I. INTRODUCTION

The existence of nanobubbles was proposed by Parker *et al.*[1] in 1994. Despite theoretical predictions,[2] they are considered as stable gaseous nanostructures on solid/liquid interfaces.[3–5] First direct observations of nanobubbles were carried out in 2000 employing tapping mode atomic force microscopy (TM AFM).[6,7] Besides the direct immersion of a substrate to a liquid, there are also more sophisticated techniques of controlled and reproducible nanobubble formation based on the solvent exchange,[8,9] thermal shocks,[10] and electrochemical generation of gases.[11–14] In the solvent exchange technique, the supersaturation of the air is induced at the interface. The substrate is first immersed into ethanol, which is known to have higher air solubility than water. Ethanol is then gently displaced by water. When the two liquids mix, the air solubility gradually decreases and an excess gas precipitates and is trapped at the interface forming detectable nanobubbles. Besides the nanobubbles, the solvent exchange technique was also successfully employed for the preparation of liquid nanodroplets.[15]

Nanobubbles were prepared and studied on highly oriented pyrolytic graphite,[6,11,13,16–24] polystyrene,[25] mica,[10,22,26] bare[27–29] and alkanethiol modified[28–31] gold, hydrophobic silicon wafers,[7,24,32–34] MoS$_2$, and talc.[35]

In this work, we study the interactions between nanobubbles with two model proteins—bovine serum albumin (BSA) and papain on Au(111) surface. We have chosen the two proteins because of their distinctly different resistance towards the protein denaturation in aqueous solutions of ethanol. While papain withstands a hostile environment of ethanol almost without structural changes,[36] BSA undergoes a strong denaturation and aggregation of its molecules even in diluted solutions[37] of ethanol.

The nanobubbles formed by the solvent exchange technique[8,9] were exposed to the aqueous solutions of the two proteins, which was followed by the solvent exchange to ethanol. While BSA was found not to protect the nanobubbles in ethanol, a considerable part of them survived the solvent exchange when papain was introduced. This distinctly different behavior of the two proteins was ascribed to their different resistance towards the protein denaturation in aqueous solutions of ethanol. The nanomorphology of the papain/nanobubble assemblies was investigated by means of atomic force lithography.[38–41]

To the best of our knowledge, there is no study dealing with gaseous nanostructures in the environment of ethanol. Here, we report on the presence of the stable air nanobubbles in ethanol, employing the double solvent exchange technique combined with the protection by papain protein. We hope that the ability to form protected nanobubbles in various liquid environments may have implications in the studies of their formation, heterogeneous catalysis, as well as in transmembrane gas transport studies.

II. EXPERIMENT

BSA (fraction V, >96%) and papain (2 × recrystallized) proteins were purchased from Sigma-Aldrich (Prague, Czech Republic) and used without any further purification. Absolute ethanol (99.8%) was obtained from AppliChem (Darmstadt, Germany). De-ionized water with a minimum resistivity of 18 MΩ cm was obtained by means of a Milli–Q RGpurification system (Millipore Co., Billerica, MA). Water solutions of BSA and papain (both at the concentration of 400 ppm) were prepared by dissolving the respective protein in de-ionized air-saturated water. Gold substrates (250 nm of gold on 1.5 nm chromium sublayer) on borosilicate glass were purchased from Arrandee (Werther, Germany). They were annealed with a butane flame on a glass-ceramic hob. After cooling, the substrates were immediately inserted into a degreased, cleaned, dried, and dust-free AFM flow liquid cell (Agilent Technologies, Santa Clara, CA).

The gold substrate was first inspected *ex situ* by the TM AFM. Afterwards, ethanol was introduced into the flow cell

a)Electronic mail: viliam.kolivoska@jh-inst.cas.cz

and the interface was reinspected *in situ* by TM AFM. Any possible surface contamination was removed by a repeated large-scale (10 μm $\times$ 10 μm) nanoshaving ("nanocleaning") employing the contact mode atomic force microscopy (CM AFM) applied either *ex situ* or in ethanol. The purity of the gold/ethanol interface was inspected 30 min later by TM AFM. Roughly 95% of the contamination was routinely removed. All subsequent observations were carried out within the nanocleaned region. Ethanol was gently replaced by water and the interface containing nanobubbles was again scrutinized *in situ* by TM AFM. Water solution of protein (either BSA or papain) was then introduced into the flow cell for 30 min. The excess protein in the bulk of the solution was subsequently removed by extensive water rinsing and the interface was reinspected *in situ* by TM AFM in pure water. Afterwards, the aqueous environment was replaced by ethanol and the interface was analyzed *in situ* by TM AFM imaging and subjected to the *in situ* atomic force lithography ("nanoshaving").

All measurements were carried out on Agilent 5500 SPM (Agilent Technologies). Except for the initial surface nanocleaning and nanoshaving performed to displace the protein layers, all other measurements were obtained by means the TM AFM technique. The magnetically coated probes ("Type II MAClevers," Agilent Technologies) were oscillated close to a resonant frequency by an external oscillating magnetic field provided by an induction coil placed directly above the probe. The nominal resonant frequency of the probe is $f_N = 75$ kHz (in the air, reference range 45–115 kHz) with the nominal force constant $k_N = 2.8$ N/m (reference range 0.5–9.5 N/m). The actual value of k was determined by recording the resonant frequency f of a probe in the air and employing the cubic interpolation in the k vs f relationship. The probe relative amplitude A_r was determined as the ratio of the set-point amplitude A maintained when imaging and the amplitude of the probe retracted from the imaged interface A_0. In our measurements, we frequently employed A_r values as high as 99% in order to reduce the interactions between the nanobubbles and the probe. Besides the topography image, cantilever deflection and friction (CM AFM) and phase shift (TM AFM) were recorded.

The nanocleaning and nanoshaving were performed in a constant repulsive force CM AFM. Prior to it, the deflection–distance spectroscopy was performed to determine the exact loading force applied. The sensitivity S of a given laser/cantilever configuration, defined as the ratio of the laser deflection D (in volts) and the cantilever deflection z (in nanometers), was determined as a slope in the repulsive part of the laser deflection–distance (D vs z) curve. The obtained value of S was employed to calculate the cantilever deflection, $\Delta z = z$(surface)$-z$(retracted probe), from the laser deflection $\Delta D = D$(surface)$-D$(retracted probe). The ΔD value was kept constant by the feedback electronics. The actual applied repulsive loading force F was calculated from Hooke's law as $F = -k\Delta z$. Typically, the values of F were in the range of 20–40 nN.

Both imaging and nanoshaving were performed with the same probe at the recording speed of 0.5–1 line/s. The AFM images shown in Sec. III are plane-corrected. The images were analyzed employing the scanning probe microscopy data visualization and analysis program Gwyddion 2.20 (Czech Metrology Institute, Brno, Czech Republic).[42–44]

III. RESULTS AND DISCUSSION

As mentioned earlier, the nanobubbles were prepared by immersing the gold substrate into ethanol, which was followed by the gentle solvent exchange to water.[8,9] Figure 1 shows the atomic force micrographs of the gold surface in the course of the nanobubble preparation. Figures 1(a) and 1(d) show the *ex situ* topography and deflection image of an annealed and nanocleaned gold substrate obtained by CM AFM in the air. One can observe grains and their boundaries that are typical for the surface of glass-supported gold substrate. The same substrate immersed in ethanol was reinspected *in situ* by TM AFM technique. The use of the flow cell allowed us to observe exactly the same position as previously inspected *ex situ*. Figures 1(b) and 1(e) show the corresponding topography and phase images in ethanol. Both show the same features as when inspected *ex situ*. Importantly, no nanobubbles are formed in ethanol. Subsequently, ethanol was gently replaced by water and scrutinized by TM
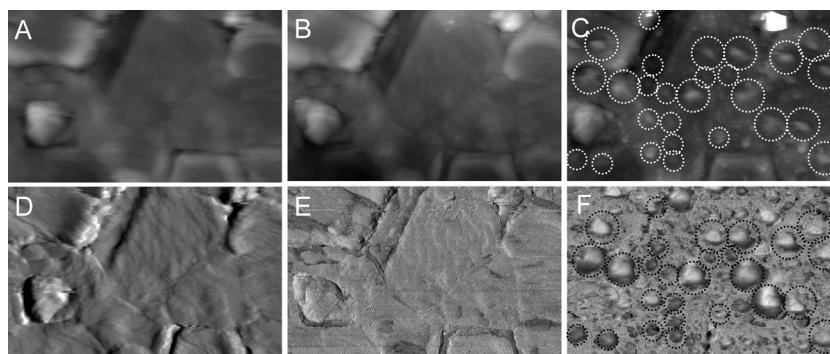

FIG. 1. Topography (a)–(c), deflection (d), and phase (e), (f) images of the gold substrate obtained in the air (a), (d), in ethanol (b), (e), and in water (c), (f). Image size: 3.2 μm $\times$ 2.0 μm, z bar is 90 nm (a)–(c), 0.24 V (d), and 40° (e), (f).

AFM again. Figures 1(c) and 1(f) show the corresponding topography and phase images in water.

Unlike in the air and ethanol, the gold surface in water is covered by nanobubbles. They appear as bright objects in the topography image [Fig. 1(c)] . Some of them are denoted by large or small white dotted circles. The nanobubbles are not strictly spherical as their imaged shape is influenced by the interactions with the probe. The phase shift between the oscillating magnetic field driving the probe and the resulting probe oscillation sensitively reflects these interactions. "Sticky" surface structures such as nanobubbles tend to retard the probe due to the adhesion forces and manifest themselves as having a negative phase shift compared to nanobubble-free regions exhibiting weaker interactions with the probe. We have employed silicon cantilevers that are known to interact with nanobubbles.[27] In the phase image obtained in water [Fig. 1(f)], small nanobubbles indeed appear as dark spheres and are denoted by small black solid circles. For larger nanobubbles (large black solid circles), only their marginal regions have a pronounced negative phase shift while the central parts appear brighter. This may be explained by the penetration of the probe into the gaseous phase[24] causing the adhesion forces to be counterbalanced. Note that most of the nanobubbles appear larger in the phase image than in the topography, which suggests that they are indeed compressed by the probe when imaged. The compressibility of nanobubbles was further confirmed in a series of experiments, in which the relative set-point amplitude A_r was gradually decreased from 95% to 70% while all other scanning parameters were kept fixed. A decrease in the relative probe amplitude leads to an increase in the pressure exerted by the probe on the sample.[16] Higher pressure causes a pronounced penetration of the probe into the gaseous phase of nanobubbles, which leads to the reduction of their imaged volume.[24] We have found that at $A_r = 70\%$ the nanobubbles apparently disappeared, as observed in the topography image, while the phase imaging clearly confirmed their presence. When the A_r value was set back to 95%, the nanobubbles reappeared. This confirms that the observed nanostructures are reversibly compressible by the scanning probe, which is a typical feature of gaseous nanobubbles.[24]

The nanobubbles were further exposed to solutions of BSA or papain. Figure 2 shows topography [Figs. 2(a)–2(c)] and phase [Figs. 2(d)–2(f)] images obtained *in situ* by TM AFM in the course of the BSA adsorption and subsequent solvent exchange to ethanol. For better orientation, the dotted rectangles denote common surface region and white arrays depict notable grain boundaries in the underlying gold substrate. Figures 2(a) and 2(d) show the topography and phase image of the gold/water interface with nanobubbles prepared by the ethanol-to-water solvent exchange, i.e., employing the same approach as in Fig. 1. Similarly, the nanobubbles appear as bright objects in topography image [Fig. 2(a)] with a negative phase shift [Fig. 2(d)]. Some of them are denoted by dotted circles. The water/gold interface was subsequently exposed to the 400 ppm solution of BSA in water for 30 min followed by extensive water rinsing.
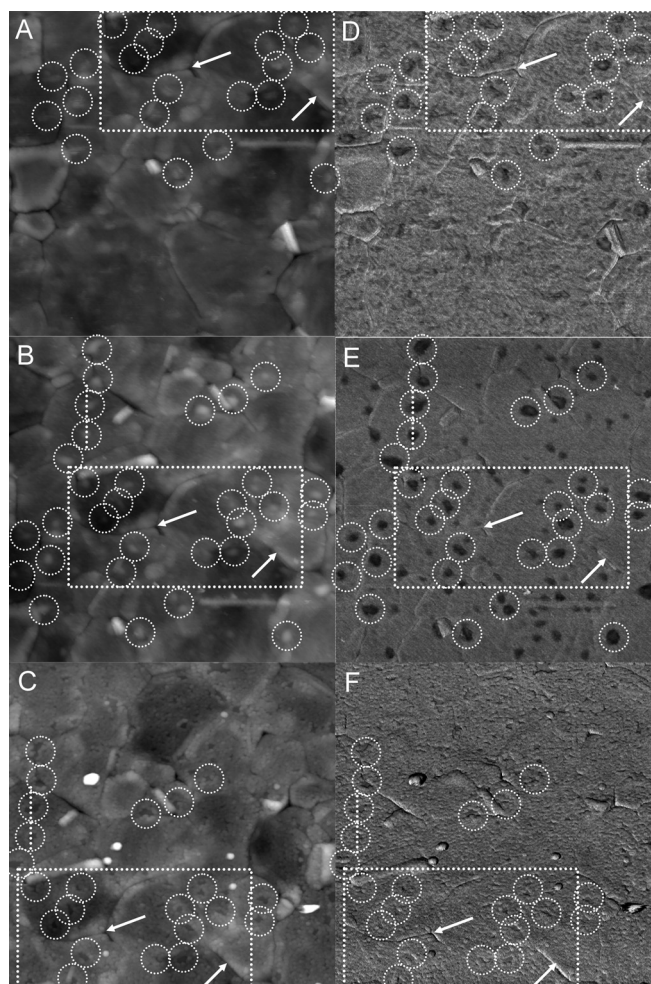

FIG. 2. Topography (a)–(c) and phase (d)–(f) images of the gold substrate obtained in water before (a), (d) and after (b), (e) the adsorption of BSA and after the solvent exchange to ethanol (c), (f). Image size: 5.0 μm × 5.0 μm; z bar is 70 nm (a)–(c) and 20° (d)–(f). Solid white vertical bars in (b), (c), (e), and (f) depict the places for the section analysis.

Figures 2(b) and 2(e) show the topography and phase image upon the protein adsorption in pure water. In the topography image [Fig. 2(b)], the nanobubbles appear at the same positions as prior to the introduction of the protein [Fig. 2(a)]. The presence of nanobubbles is well discernible by the phase imaging [Fig. 2(e)]. The aqueous environment was subsequently replaced by ethanol and reinspected by *in situ* TM AFM. Figures 2(c) and 2(f) show the corresponding topography and phase image in ethanol.

The nanomorphology of the interface has changed with the roughness being apparently increased. The locations occupied by nanobubbles in the aqueous environment become bare in ethanol [compare the circles in Figs. 2(b) and 2(c)]. The phase imaging in Fig. 2(f) shows no domains with distinctly negative phase shift, suggesting the absence of nanobubbles in ethanol.

Figure 3 shows the results of the section analysis of the images in Figs. 2(b), 2(c), 2(e), and 2(f). The corresponding section line is denoted in the panels in Fig. 2 by the solid vertical white bar.
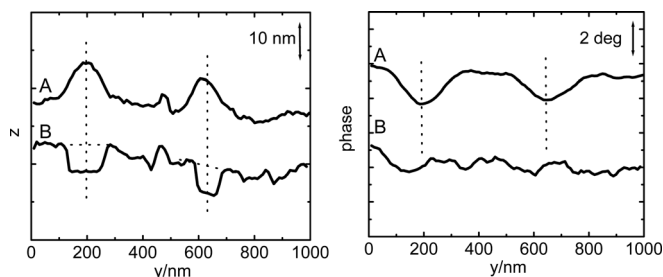
FIG. 3. Topography (left panel) and phase (right panel) profile obtained in water after the adsorption of BSA (a) and after the solvent exchange to ethanol (b). Profiles are vertically shifted for clarity. The vertical dotted lines denote the positions of nanobubbles in water.

The nanobubbles in water (at ≈ 200 and ≈ 630 nm in line A in the left panel) correspond to the holes in the BSA film in ethanol (profile B in the left panel). This suggests that the BSA molecules adsorb everywhere except the places where nanobubbles are present. When water is replaced by ethanol, the nanobubbles dissolve. The BSA film in ethanol contains vacancies at locations previously occupied by nanobubbles in the aqueous environment. This is also confirmed by the phase profile (right panel). In water, the positions at ≈ 200 and ≈ 630 nm (line A) clearly show a negative shift confirming the presence of nanobubbles. On the other hand, no negative phase shift is observed in ethanol (line B). This confirms that nanobubbles do not survive in ethanol.

The holes in the BSA film in ethanol [Fig. 2(c)] were further subjected to the statistical analysis. Figure 4 shows the histogram of the depth values constructed for 40 holes in the BSA film in ethanol. The average value is 6.8 ± 1.4 nm. This value is equal to the film thickness, provided that the bottom of the hole coincides with surface of the gold substrate. We note that the obtained film thickness value is on the order of dimensions of a single BSA molecule (14 nm $\times 4$ nm $\times 4$ nm).[45]

In conclusion, the adsorption of BSA molecules at gold/water interface containing nanobubbles does not significantly affect their detectability by the TM AFM technique. Importantly, the presence of the BSA film does not change their occurrence and positions. This suggests that the BSA molecules cannot displace nanobubbles from their positions
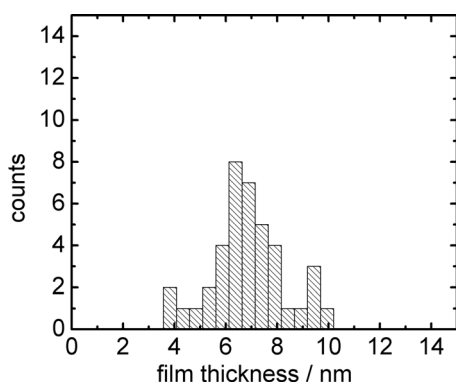

FIG. 4. Histogram of the BSA film thickness values constructed from the measurement of depth values of 40 holes in the film.

and adsorb only at the rest of the interface. The nanomorphology of the interface changes abruptly when the aqueous environment is exchanged by ethanol. All nanobubbles dissolve leaving behind the BSA film with vacancies at positions previously occupied by nanobubbles in the aqueous environment. The dissolution of nanobubbles in ethanol can be rationalized by the fact that solubility of the air is higher in ethanol than in water. As all nanobubbles vanish in ethanol when BSA is present, this protein does not act as a protective agent that would stabilize them in this environment.

The approach applied in the experiments with BSA was also utilized in the case of papain. The nanobubbles were formed at gold/water interface by means of the ethanol-to-water exchange[8,9] and their presence in the aqueous environment was confirmed by TM AFM both before and after the introduction of papain. Similar to BSA, the presence of papain was found not to affect the occurrence and positions of nanobubbles. The aqueous environment was then replaced by ethanol. Figures 5(a) and 5(c) show the topography and phase images obtained in ethanol immediately upon the water-to-ethanol exchange. The nanomorphology of the papain film is similar to that of BSA. The film contains vacancies [solid circles in Fig. 5(a)], the position of which corresponds to the presence of nanobubbles in the aqueous environment. The phase image shows no negative phase shift at these positions [solid circles in Fig. 5(c)], confirming that no nanobubbles survived here. However, there are also bright features in the topography [dotted circles in Fig. 5(a)] with corresponding negative values of the phase shift [dotted
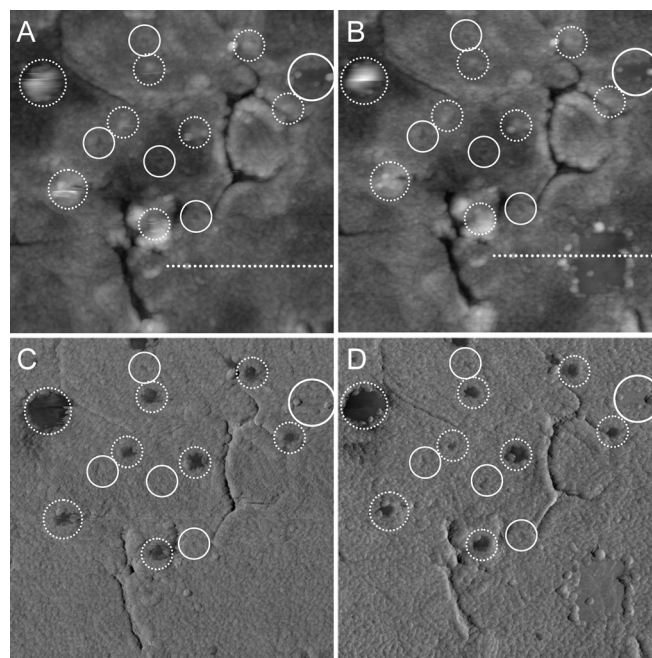

FIG. 5. Topography (a), (b) and phase (c), (d) images of the papain film on gold in ethanol obtained immediately upon the solvent exchange (a), (c) and after 1 h and nanoshaving (0.5 μm $\times 0.5$ μm) in the lower right part of the image (b), (d). Image size: 3.7 μm $\times 3.7$ μm, z bar is 70 nm (a), (b) and 40° (c), (d). Solid white horizontal bars in (a) and (b) depict the places for the further section analysis.

circles in Fig. 5(c)]. Obviously, these objects behave in the same way as in the aqueous environment. Therefore, we suggest that these objects are nanobubbles that survived the water-to-ethanol exchange and are stable in ethanol. As mentioned earlier, the dissolution of the nanobubbles in the course of the water-to-ethanol can be explained by an increase in the air solubility in the latter environment. However, papain, unlike BSA, prevents the dissolution of a part of nanobubbles.

The papain/nanobubble assembly in ethanol shown in Figs. 5(a) and 5(c) was further reinspected 1 h upon its formation [Figs. 5(b) and 5(d)]. In the meantime, the probe was scanned over the square area of dimensions 0.5 μm $\times$ 0.5 μm in the CM AFM regime (nanoshaving). This was performed to remove the papain film and regenerate the pure gold substrate under existing *in situ* conditions. The applied repulsive force of 21 nN was found to be sufficiently high to displace the papain film and reveal the gold surface. In a blank experiment with the same probe and configuration at pure gold/ethanol interface, we have found that this action does not damage the underlying gold substrate for repulsive forces up to 400 nN. The removed material is therefore the protein film and not the underlying gold substrate.

The nanoshaving formed the square region of pure gold observable in the lower right part of the micrographs shown in Figs. 5(b) and 5(d). Note that the phase shift [Fig. 5(d)] of the region of pure gold created artificially is the same as that of natural vacancies in the papain film caused by the dissolution of nanobubbles [see the big solid white circle in Fig. 5(d)]. On the contrary, the regions pertaining to surviving nanobubbles have distinctly negative phase shift compared to the nanoshaved area, confirming a pronounced adhesion between the probe and surviving nanobubbles.

Apart from the region subjected to the nanoshaving, the image of the interface obtained 1 h upon the formation [Figs. 5(b) and 5(d)] exhibits exactly the same features as that obtained immediately [Figs. 5(a) and 5(c)]. This clearly confirms that surviving nanobubbles as well as the papain film are stable in ethanol for at least 1 h.

The question remains why some nanobubbles survive in ethanol when papain is used while all of them dissolve when BSA is introduced. To find the answer, we have further analyzed the nanomorphology of papain film in ethanol. Figure 6(a) shows the results of the section analysis through the nanoshaved area [see the white solid horizontal bars in Figs. 5(a) and 5(b)] performed before [dotted profile in Fig. 6(a)] and after [solid profile in Fig. 6(a)] the nanoshaving.

The profile shown in Fig. 6(a) is one of twenty employed to determine the average thickness of the papain film in ethanol based on the nanoshaving. The corresponding histogram is shown in Fig. 6(b) with the average value equal to 7.2 $\pm$ 1.1 nm. The average thickness of the papain film was also evaluated from the depth of naturally occurring holes that correspond to dissolved nanobubbles. Due to a relatively scarce occurrence of holes in the micrograph shown in Fig. 5, we have also taken into account micrographs obtained at other positions of the same sample (not shown). The aver-
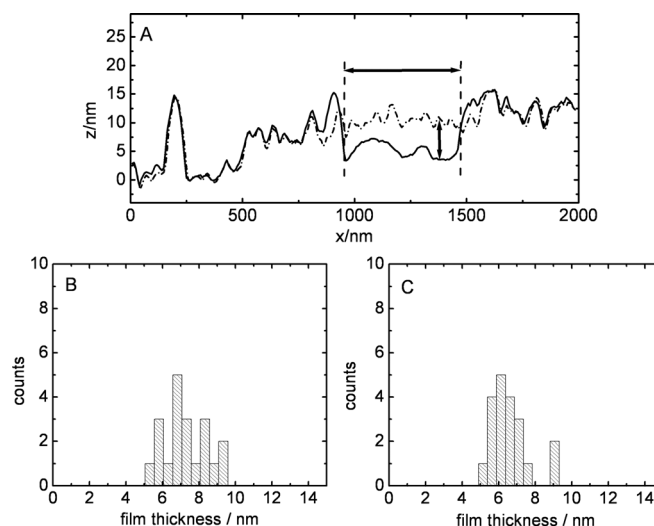

FIG. 6. Section analysis of the papain film in ethanol performed before (dashed line) and after (solid line) the nanoshaving (a). (b), (c) The histograms of the film thickness constructed from 20 measurements determined by nanoshaving (b) and depth measurements of natural holes in the papain film (c).

age value of the film thickness obtained by the depth measurements is 6.6 $\pm$ 1.1 nm [histogram shown in Fig. 6(c)] and agrees well with the value found by the nanoshaving. These two values do not significantly differ from that for BSA (6.8 $\pm$ 1.4 nm, Fig. 4) suggesting that the two protein films have practically the same thickness in ethanol.

The layer thickness determination also allows one to estimate the surface coverage of the proteins. The molar mass of the protein is $M_{BSA} = 67$ kg/mol and $M_{papain} = 23$ kg/mol. If one assumes the density of the interfacial layers to be ~ 1 g/cm^3, the respective surface coverages are approximately $\Gamma_{BSA} = 1.0 \times 10^{-11}$ mol/cm^2 and $\Gamma_{papain} = 2.2 \times 10^{-11}$ mol/cm^2. The value obtained for BSA is smaller than that for papain, which corresponds to the different size of respective molecules. We assume that both proteins form monolayers at the interface as the thickness of their films is comparable to dimensions of their molecules [14 nm $\times$ 4 nm $\times$ 4 nm for BSA (Ref. 45) and 7 nm $\times$ 5 nm $\times$ 3 nm for papain (Ref. 46)].

As the two proteins form films with nearly the same thickness, the reason why they behave differently with respect to the nanobubble stabilization in ethanol cannot lie in their distinctly different nanomorphology.

Generally, proteins are known to adsorb at the air/water interfaces.[47] One can therefore assume that the protein molecules adsorb not only at the gold/water interface but also at the nanobubble/water interface. It is important to note that prior to water-to-ethanol exchange, the excess protein in the bulk of the solution was removed by water rinsing. Therefore, only the adsorbed protein is present in the system when the solvent exchange is performed. During its course, the denaturation of the proteins may take place. Unfortunately, AFM techniques are not sensitive enough to determine to what extent this proceeds. Therefore, we follow the works on the BSA and papain denaturation in the aqueous solutions of ethanol. Szabó *et al.*[36] measured the catalytic activity of

papain in water/ethanol mixtures of variable composition. They found that even in 90% ethanol papain retains as much as 75% of its catalytic activity obtained in pure water. Therefore, the papain molecules do not undergo significant structural changes even when in concentrated ethanol. On the other hand, Liu *et al.*[37] revealed that BSA denaturation takes place in the solutions of ethanol. Ethanol is more hydrophilic than the BSA molecules. When increasing the concentration of ethanol, the solvation sphere around the BSA molecules gradually disappears.[37] If the concentration of ethanol is less than 20%, the hydrophobic tryptophan residues are located in the molecular core, as observed by fluorescence spectroscopy.[37] For the ethanol concentration falling into the range 20%–40%, the deformation of BSA molecules occurs and some of tryptophan moieties become exposed to the liquid phase. Above 40% of ethanol, the strong BSA denaturation takes place.[37]

This helps us to rationalize why papain is able to protect nanobubbles from being dissolved in the course of the solvent exchange while BSA is not. As mentioned earlier, both proteins are assumed to form a layer on top of nanobubbles in water.[47] The structure of the papain layer does not change much during the water-to-ethanol exchange as it is stable in concentrated solutions of ethanol and perhaps also in pure ethanol. The papain film retains its ability to create a physical barrier that hinders the mass transfer of the air molecules from the nanobubble to the bulk of ethanol raising the chance for the nanobubbles to survive in ethanol. On the other hand, though BSA film covers and protects the nanobubbles in water, it undergoes structural changes in the course of water-to-ethanol exchange due to the protein denaturation. Vacancies are created in the BSA film and allow the mass transfer of the air molecules to ethanol to take place, which ultimately leads to the dissolution of all present nanobubbles.

Figure 7 shows a general picture of how the nanobubbles form on gold surface and interact with the two protein films. First, the dry gold substrate is immersed in ethanol, where no nanobubbles are formed [Fig. 7(a)]. Ethanol is then gently displaced by water. The solubility of the air is lower in water than in ethanol. Therefore, a part of the air molecules

formerly dissolved in ethanol precipitates in the course of the solvent exchange to water.[3] The formed nanobubbles are trapped by the gold/water interface [Fig. 7(b)]. The interface is then exposed to the solutions of either BSA or papain. The protein molecules adsorb at the gold/water as well as the nanobubble/water interface [Fig. 7(c)]. Excess protein is removed from the bulk of the solution by water rinsing [Fig. 7(d)]. The interface is fully covered by the protein layer. Aqueous environment is then replaced by ethanol. In the case of BSA, the protein film denaturates and changes its structure. Holes created in the film are detrimental to the nanobubbles as they allow the mass transport of the gas to the ethanol bulk, which ultimately causes the dissolution of all nanobubbles [left panel of Fig. 7(e)]. On the contrary, no severe structural changes occur in the papain film during the water-to-ethanol exchange. Therefore, there is an increased chance for the papain film to prevent the gas transport and to protect the nanobubbles from being dissolved in ethanol. Some of the nanobubbles therefore survive even in pure ethanol [right panel of Fig. 7(e)].

IV. SUMMARY AND CONCLUSIONS

Interfacial ambient gas nanobubbles were prepared at gold/water interface by means of the ethanol-to-water solvent exchange technique. The presence of nanobubbles was confirmed by the TM AFM technique both before and after the introduction of either BSA or papain protein. The two protein films do not influence the occurrence and positions of interfacial nanobubbles. Upon the solvent exchange to ethanol, the fate of the nanobubbles was found to strongly depend on which protein was introduced. The presence of the BSA film at the interface does not protect the nanobubbles from being dissolved in ethanol. Nanobubbles leave behind the BSA film with the vacancies corresponding to their positions in the aqueous environment. On the other hand, the papain film protects some of the nanobubbles from dissolution in ethanol. An enhanced protecting power of papain was explained by its ability to withstand the protein denaturation in concentrated aqueous solutions of ethanol.

The gold substrate, either genuine or modified, frequently serves as an interface, at which the processes of biological interest takes place. Tailored self-assembled monolayers of thiolate molecules adsorbed at gold/liquid interface promote or resist the protein adsorption and the cell growth. The work presented here suggests that gaseous nanostructures naturally occurring at gold/water interface—the nanobubbles—are important factors that contribute to its morphology. Subsequently, they can affect the processes in which the interfacial proteins play a key role. A part of an interface occupied by the nanobubbles can become silent in experiments, which can cause errors in the quantitative and/or qualitative analysis. Knowledge of the interactions of nanobubbles with the proteins might be generally exploited in the studies of the cell adhesion and growth at solid/liquid interfaces. Moreover, as shown earlier, understanding the interactions between the nanobubbles and proteins might help to
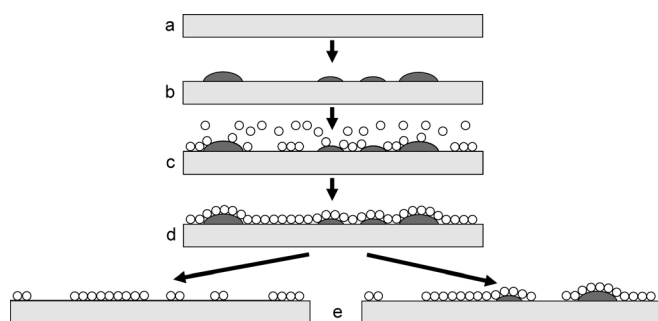

FIG. 7. Schematic representation of the nanobubble formation on gold surfaces and the interactions with BSA and papain films. Gold surface in contact with ethanol (a), water (b), solution of protein (c), after rinsing by water (d), and in ethanol when BSA [(e), left] and papain [(e), right] were previously introduced.

develop and tune the nanobubble-based cleaning procedures, e.g., by electrochemically generated nanobubbles.

[1] J. L. Parker, P. M. Claesson, and P. Attard, J. Phys. Chem. **98**, 8468 (1994).

[2] S. Ljunggren and J. Ch. Eriksson, Colloids Surf., A **129**, 151 (1997).

[3] V. S. J. Craig, Soft Matter **7**, 40 (2011).

[4] B. M. Borkent, S. M. Dammer, H. Schonherr, G. J. Vancso, and D. Lohse, Phys. Rev. Lett. **98**, 204502 (2007).

[5] W. A. Ducker, Langmuir **25**, 8907 (2009).

[6] S. T. Lou, Z. Q. Ouyang, Y. Zhang, X. J. Li, J. Hu, M. Q. Li, and F. J. Yang, J. Vac. Sci. Technol. B **18**, 2573 (2000).

[7] N. Ishida, T. Inoue, M. Miyahara, and K. Higashitani, Langmuir **16**, 6377 (2000).

[8] S. T. Lou, J. X. Gao, X. D. Xiao, X. J. Li, G. L. Li, Y. Zhang, M. Q. Li, J. L. Sun, and J. Hu, Chin. Phys. **10**, S108 (2001).

[9] S. T. Lou *et al.*, Mater. Charact. **48**, 211 (2002).

[10] X. H. Zhang, X. D. Zhang, S. T. Lou, Z. X. Zhang, J. L. Sun, and J. Hu, Langmuir **20**, 3813 (2004).

[11] L. J. Zhang, Y. Zhang, X. H. Zhang, Z. X. Li, G. X. Shen, M. Ye, C. H. Fan, H. P. Fang, and J. Hu, Langmuir **22**, 8109 (2006).

[12] G. Liu, Z. H. Wu, and V. S. J. Craig, J. Phys. Chem. C **112**, 16748 (2008).

[13] Z. H. Wu, H. Chen, Y. M. Dong, H. L. Mao, J. Sun, S. Chen, V. S. J. Craig, and J. Hu, J. Colloid. Interface Sci. **328**, 10 (2008).

[14] S. Yang, P. Tsai, E. S. Kooij, A. Prosperetti, H. J. W. Zandvliet, and D. Lohse, Langmuir **25**, 1466 (2009).

[15] X. H. Zhang and W. Ducker, Langmuir **23**, 12478 (2007).

[16] P.Janda, O. Frank, Z. Bastl, M. Klementová, H., Tarábková, and L., Kavan, Nanotechnology **21**, 095707 (2010).

[17] Z. H. Wu, X. H. Zhang, X. D. Zhang, J. L. Sun, Y. M. Dong, and J. Hu, Chin. Sci. Bull. **52**, 1913 (2007).

[18] X. H. Zhang, G. Li, N. Maeda, and J. Hu, Langmuir **22**, 9238 (2006).

[19] L. Zhang, X. H. Zhang, C. Fan, Y. Zhang, and J. Hu, Langmuir **25**, 8860 (2009).

[20] B. M. Borkent, S. de Beer, F. Mugele, and D. Lohse, Langmuir **26**, 260 (2010).

[21] X. H. Zhang, N. Maeda, and J. Hu, J. Phys. Chem. B **112**, 13671 (2008).

[22] L. Zhang, X. H. Zhang, Y. Zhang, J. Hu, and H. Fang, Soft Matter **6**, 4515 (2010).

[23] X. H. Zhang, A. Kumar, and P. J. Scales, Langmuir **27**, 2484 (2011).

[24] X. H. Zhang, N. Maeda, and V. S. J. Craig, Langmuir **22**, 5025 (2006).

[25] Y. Wang, B. Bhushan, and X. Zhao, Langmuir **25**, 9328 (2009).

[26] Z. H. Wu, X. H. Zhang, X. D. Zhang, G. Li, J. Sun, Y. Zhang, M. Li, and J. Hu, Surf. Interface Anal. **38**, 990 (2006).

[27] M. Holmberg, A. Kühle, J. Garnæs, K. A. Mørch, and A. Boisen, Langmuir **19**, 10510 (2003).

[28] H. Seo, M. Yoo, and S. Jeon, Langmuir **23**, 1623 (2007).

[29] H. Seo, N. Jung, D. Lee, and S. Jeon, Colloids Surf., A **336**, 99 (2009).

[30] X. H. Zhang, Phys. Chem. Chem. Phys. **10**, 6842 (2008).

[31] B. Song, W. Walczyk, and H. Schönherr, Langmuir **27**, 8223 (2011).

[32] J. Yang, J. Duan, D. Fornasiero, and J. Ralston, J. Phys. Chem. B **107**, 6193 (2003).

[33] S. Darwich, K. Mougin, L. Vidal, E. Gnecco, and H. Haidara, Nanoscale **3**, 1211 (2011).

[34] N. Ishida and H. Higashitani, Minerals Engineering **19**, 719 (2006).

[35] X. H. Zhang and N. Maeda, J. Phys. Chem. C **115**, 736 (2011).

[36] A. Szabó, M. Kotormán, I. Laczkó, and M. Simon, J. Mol. Catal. B-Enzym. **41**, 43 (2006).

[37] R. Liu, P. Qin, L. Wang, X. Zhao, Y. Liu, and X. Hao, J. Biochem. Mol. Toxicol. **24**, 66 (2010).

[38] G. Liu, S. Xu, and Y. Qian, Acc. Chem. Res. **33**, 457 (2000).

[39] P. M. Mendes, C. L. Yeung, and J. A. Preece, Nanoscale Res. Lett. **2**, 373 (2007).

[40] E. Pişkin, Hacettepe J. Biol. Chem. **35**, 157 (2007).

[41] L. G. Rosa and J. Liang, J. Phys.: Condens. Matter. **21**, 483001 (2009).

[42] P. Klapetek, D. Nečas, A. Campbellová, A. Yacoot, and L. Coenders, Meas. Sci. Technol. **22**, 025501 (2011).

[43] P. Klapetek, I. Ohlídal, D. Franta, A. Montaigne-Ramil, A. Bonanni, D. Stifter, and H. Sitter, Acta Phys. Slov. **53**, 223 (2003).

[44] P. Klapetek and I. Ohlídal, Ultramicroscopy **94**, 19 (2003).

[45] A. K. Wright and M. R. Thompson, Biophys. J. **15**, 137 (1975).

[46] R. W. Pickersgill, G. W. Harris, and E. Garman, Acta Crystallogr., Sect. B: Struct. Sci. **B48**, 59 (1992).

[47] A. W. Adamson and A. P. Gast, *Physical Chemistry of Surfaces*, 6th ed. Wiley, New York, 1997 p. 542.